Spectral Tuning of Deep Red Cone Pigments[†]

Tabitha L. Amora,[‡] Lavoisier S. Ramos,[‡] Jhenny F. Galan, and Robert R. Birge*

Departments of Chemistry and of Molecular and Cell Biology, University of Connecticut, 55 North Eagleville Road, Storrs, Connecticut 06269

Received October 15, 2007; Revised Manuscript Received February 8, 2008

ABSTRACT: Visual pigments are G-protein-coupled receptors that provide a critical interface between organisms and their external environment. Natural selection has generated vertebrate pigments that absorb light from the far-UV (360 nm) to the deep red (630 nm) while using a single chromophore, in either the A1 (11-*cis*-retinal) or A2 (11-*cis*-3,4-dehydroretinal) form. The fact that a single chromophore can be manipulated to have an absorption maximum across such an extended spectral region is remarkable. The mechanisms of wavelength regulation remain to be fully revealed, and one of the least well-understood mechanisms is that associated with the deep red pigments. We investigate theoretically the hypothesis that deep red cone pigments select a 6-*s*-*trans* conformation of the retinal chromophore ring geometry. This conformation is in contrast to the 6-*s*-*cis* ring geometry observed in rhodopsin and, through model chromophore studies, the vast majority of visual pigments. Nomographic spectral analysis of 294 A1 and A2 cone pigment literature absorption maxima indicates that the selection of a 6-*s*-*trans* geometry red shifts M/LWS A1 pigments by ~1500 cm^{-1} (~50 nm) and A2 pigments by ~2700 cm^{-1} (~100 nm). The homology models of seven cone pigments indicate that the deep red cone pigments select 6-*s*-*trans* chromophore conformations primarily via electrostatic steering. Our results reveal that the generation of a 6-*s*-*trans* conformation not only achieves a significant red shift but also provides enhanced stability of the chromophore within the deep red cone pigment binding sites.

Visual pigments are responsible for mediating vision and color discrimination. These pigments are members of the G-protein-coupled receptor (GPCR)[1] family, having seven transmembrane α helices as the core structure. The visual pigments in the retina are classified according to sequence similarity into mid- and long-wavelength sensitive, M/LWS (>510 nm); short-wavelength sensitive set 1, SWS1 (350–450 nm); short-wavelength sensitive set 2, SWS2 (440–461 nm); rhodopsins, RH1 (470–500 nm), and rhodopsin-like cone pigments, RH2 (460–510 nm) (*1, 2*) (Figure 1). These pigments contain a protein called opsin and a retinal chromophore, which is a derivative of vitamin A. The chromophore in vertebrate visual pigments is either 11-*cis*-retinal (an A1 retinal) or 11-*cis*-3,4-dehydroretinal (an A2 retinal) chromophore (Figure 2). The A2 retinal extends the π system by one double bond inside the ring and absorbs at longer wavelengths than the A1 retinal (*3, 4*).

Spectral tuning of visual pigments allows vertebrates to adjust visual acuity to suit their environment. Because red−green light is preferentially transmitted near the surface of the water (*5*), most freshwater fish and amphibians select an A2 retinal chromophore to extend visual sensitivity to longer wavelengths (*2, 6*). A variety of tuning mechanisms relevant to both A1 and A2 chromophores have been proposed. Electrostatic chromophore−protein interactions represent the most extensively studied mechanisms because the protein-bound chromophore is positively charged (*7–13*). The exceptions are the UV-cone pigments, which have a deprotonated Schiff base chromophore (*14–16*). The absorption spectrum of the chromophore is also sensitive to the conformation of the chromophore, and it has long been known that the selection of a 6-*s*-*trans* chromophore conformation will red shift the chromophore (*11*). The origin of this red shift is the enhanced planarity of the π system of the 6-*s*-*trans* conformation, which decreases the energy of the lowest unoccupied molecular orbital (*11*). Indeed, a 6-*s*-*trans* ring conformation was first proposed by Chen and co-workers as a spectral tuning mechanism in iodopsin (λ_{max} = 571 nm) (*17*). More recently, Makino and co-workers tested this hypothesis by incorporating locked 6-*s*-*cis*,9-*cis* retinal analogues into bleached salamander, squirrel, monkey red, and monkey green cone pigments (*18*). Their study, however, concluded that the differences in λ_{max} between the red- and green-absorbing pigments do not depend upon the conformation of the C_6-C_7 bond of the retinal. We revisit this conformational mechanism in the present paper by examining different chromophore binding site models and homology models of M/LWS pigments. We demonstrate that deep red

[†] This work was supported in part by the National Institutes of Health (NIH, GM-34548) and the National Science Foundation (NSF, BES-0412387). Computational facilities were supported by the Harold S. Schwenk Sr. Distinguished Chair in Chemistry at the University of Connecticut.

* To whom correspondence should be addressed. Telephone: 860-486-6720. Fax: 860-486-2981. E-mail: rbirge@uconn.edu.

[‡] These two authors contributed equally to this work.

[1] Abbreviations: GPCR, G-protein-coupled receptor; M/LWS, mid- and long-wavelength sensitive; DFT, density functional theory; MNDO−PSDCI, molecular neglect of differential overlap with partial single- and double-configuration interaction; BLOSUM62, block substitution matrix 62; BLAST, basic local alignment and search tool; CAChe, computer-aided chemistry; MM2, molecular mechanics 2; ABNR, adopted basis Newton−Raphson; CHARMm, chemistry at Harvard molecular mechanics; MD, molecular dynamics.

10.1021/bi702069d CCC: $40.75
Published on Web 03/28/2008

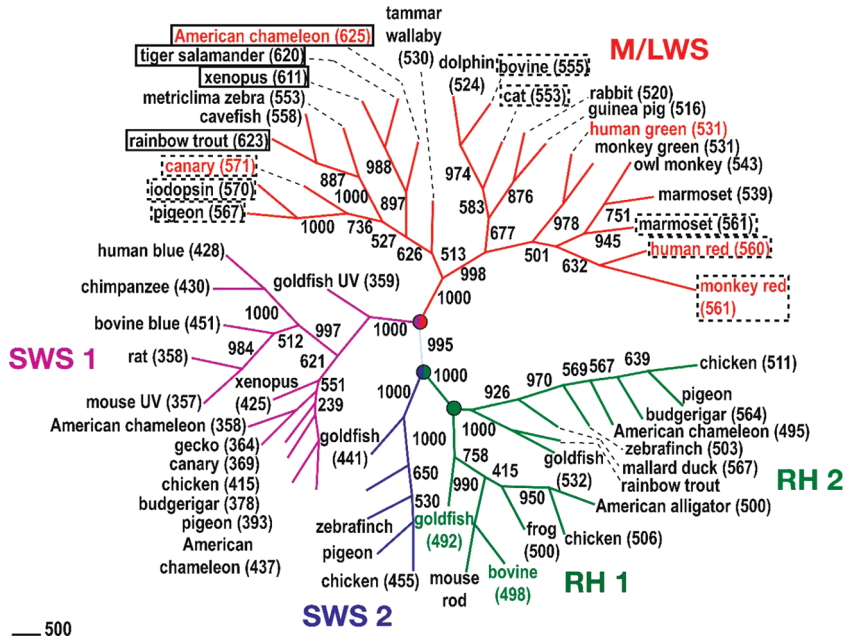

FIGURE 1: This study's premise is that many of the deep red cones are bathochromically shifted to higher wavelength by adopting a 6-*s*-*trans* conformation of the 11-*cis*-retinal chromophore. The figure places solid rectangles around those pigments for which A2 6-*s*-*trans* conformations are predicted, with dashed lines indicating more tentative assignments for the A1 6-*s*-*trans* pigments. The phylogenetic tree shown here is constructed from aligned sequences by neighbor-joining methods through ClustalW. The distances of the sequences are estimated on the basis of the Dayhoff PAM matrix by Prodist of the PHYLIP program (version 3.65). The numbers along the branches indicate the clustering percentage obtained from 1000 bootstrap resamplings. The values enclosed in parentheses are the observed absorption maxima of the pigments, when available. Classification nodes are marked with circles, and the seven pigments modeled in this study are labeled in color.

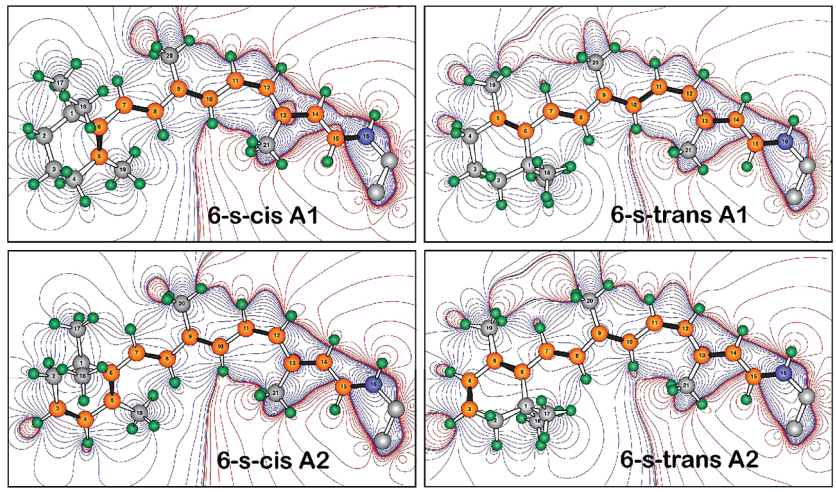

FIGURE 2: Vertebrate visual pigments select either A1 retinal or A2 (3,4-dehydroretinal) 11-*cis*-retinal as the bound chromophore. A2 retinal has an additional double bond in the β-ionone ring, which red shifts the absorption spectrum. The contours describe the differential electrostatic field based on the point-charge Mulliken population [B3LYP/6-31G(d)]. The red contours indicate areas of positive charge, and the blue contours indicate areas of negative charge relative to the chromophore as a whole, which carries a net positive charge. Note that the 6-*s*-*trans* conformers move positive charges toward the ring relative to the 6-*s*-*cis* conformers.

cones preferentially select a 6-*s*-*trans* conformer and that this selection is directly responsible for as much as a 100 nm red shift in the A2 red cone pigments. The evidence for A1 6-*s*-*trans* pigments is less compelling but warrants additional study.

Although the M/LWS pigments contain a protonated Schiff base and high binding site similarity across species, the reported absorption maxima of the vertebrate M/LWS opsins populate distinct regions of the spectrum (Figure 3). The A2 pigments provide the most dramatic example, with the vast majority near 532 or 620 nm, with only a small number in between. The A1 pigments populate three differentiated regions, with maxima at 520, 533, and 564 nm, and are a more complicated group to analyze. Our initial structure–function studies of these groupings sought differences in the amino acid residues in or near the binding site. We found no systematic changes in binding site residues that could account realistically for the dramatic differentiation depicted in Figure 3. Other studies have confirmed the lack of obvious residue-based mechanisms (*18*). We propose that the regional differences are due to chromophore conformer selection, a more subtle wavelength mechanism that can be triggered by modest changes in the binding site, as we explore below.

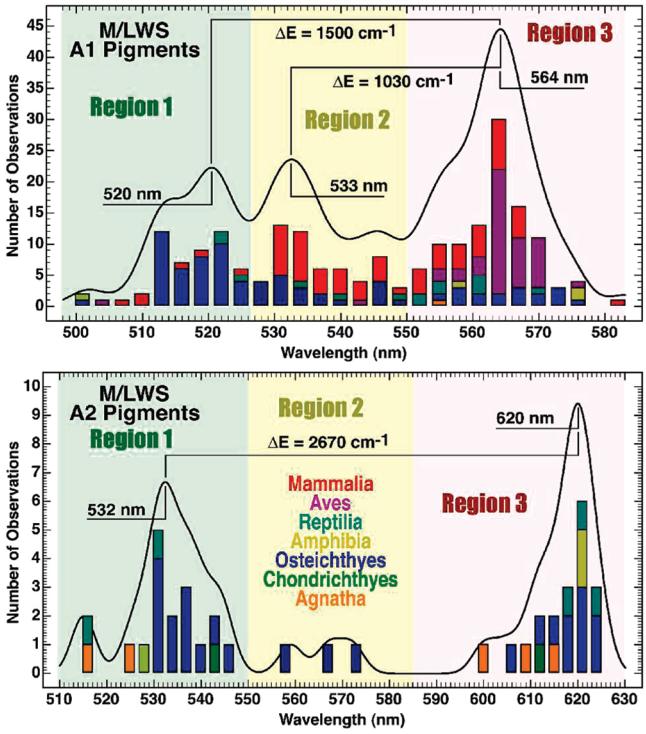

FIGURE 3: Histogram analysis of 294 M/LWS pigments reveals the distribution of absorption maxima into two or three regions of the visible spectrum for A1 (top) and A2 (bottom) pigments. We refer to those red cones with absorption maxima in region 3 as "deep red" cones and propose that these pigments have 6-*s*-*trans* chromophores. The literature data and associated references are listed in Tables S1 and S2 of the Supporting Information.

MATERIALS AND METHODS

Chromophore Binding Site Models. The isolated chromophore models that we used to examine the effect of 6-*s*-*cis* versus 6-*s*-*trans* conformation on the electronic properties of the isolated chromophores are shown in Tables S3 and S4 of the Supporting Information. The ground-state geometries of the models were minimized by DFT (B3LYP/6-31G(d)) methods in Gaussian 03 (*19*). The excited-state (spectroscopic) properties were calculated using the MNDO−PSDCI theory including full single- and double-configuration interaction within the chromophore π system (*15, 20–22*).

Homology Modeling of M/LWS Pigments of Different Vertebrates. We constructed homology models of the following seven proteins referenced via accession number: P14592 (American chameleon red, 625 nm), CAB91996 (canary red, 571 nm), AAC12941 (dolphin green, 524 nm), AAA49169 (goldfish green, 532 nm), NP_000504 (human green, 531 nm), NP_06445 (human red, 560 nm), and AAD40324 (monkey red, 560 nm). The sequences of M/LWS pigments of different vertebrates were aligned against the sequence of rhodopsin [Protein Data Bank (PDB) code 1U19] (*23*) using the BLOSUM62 scoring matrix in *MathScriptor* (www.mathscriptor.org). Hydrogen atoms were added, and an initial minimization was executed in CAChe (Fujitsu, Inc., Beaverton, OR) by MM2 methods (*24, 25*). All hydrogen atoms were minimized fully prior to optimization of the whole protein, and the backbone was locked during these minimizations. To create models with a 6-*s*-*trans* retinal chromophore, the dihedral angle of the ring was altered to change the ring conformation of the retinal.

The models were further optimized by adopted basis Newton–Raphson (ABNR) methods, with harmonic constraints on the backbone and dihedral constraints on the chromophore polyene chain using CHARMM (*26, 27*). The parameters for the chromophore were adapted from the optimized retinal structure by Hermone and Kuczera (*28*). The system was gradually heated from 0 to 300 K over an interval of 20 ps, followed by 50 ps of simulation at 300 K to equilibrate the system. All molecular dynamics (MD) simulations were carried out for 2 ns, with a time step of 0.001 ps, assuming a dielectric constant of 1.0. A nonbonded cutoff of 15 Å with a nonbonding smoothing function applied between 11 and 14 Å was used for all calculations. All MD simulations were carried out using the Charmm22 parameter proteins and TIP3P waters (*26, 27*).

Monkey red models were also generated on the basis of the human red pigments. We included in this study both 9-*cis* and 11-*cis* chromophores to better understand the relationship between this theoretical investigation and the previous experimental study by Makino et al. (*18*).

RESULTS

Chromophore Binding Site Models. The ground- and excited-state properties of the 10 sets of binding site models were calculated, and their properties are summarized in Tables S3 and S4 in the Supporting Information. The molecular diagram that is shown to the left of the data (Tables S3 and S4 in the Supporting Information) shows the geometry of the chromophore with the lowest energy conformation. A few of our models contain a protonated Schiff base without a negative counterion, while the remainder contains a negatively charge species near the Schiff base present either as a carboxylate ion group or a perchlorate ion. We have also constructed a binding site model with a total charge of −1 by introducing a carboxylate ion group and a model with a total charge of +1 by adding an iminium ion near the polyene chain of the retinal. In general, protonated Schiff bases without negative counterions select the 6-*s*-*trans*. Most others select 6-*s*-*cis*.

Homology Models. To examine the sequence similarity among M/LWS pigments, a number of vertebrate pigments were aligned with respect to the rhodopsin crystal structure (PDB code 1U19). As observed in previous studies, we identified no charged residues within 5 Å of the chromophore other than the primary counterion (*29, 30*). We also examined the residues at positions 164, 261, and 269 (rhodopsin numbering). A hydroxyl-containing residue at these positions has been shown to red shift the absorption maxima (*30, 31*). However, we observe that many of the region 1 pigments also contain Tyr, Thr, and Ser at these positions, indicating that these particular residues are not the primary source of the red shift. A summary of our findings for selected region 1 and 3 pigments is shown in Tables S5 in the Supporting Information. We conclude that serine at position 164 may play a small role in enhancing the region 1−3 shift, but this residue is not a primary source of the significant red shift. The mechanism that we propose here is the selection of a 6-*s*-*trans* chromophore conformation in the deep red (region 3)

pigments. Because this selection would be a discontinuous conformational change, a large shift in the nomographic spectral distribution would be anticipated. That feature is observed for the A2 chromophores (Figure 3).

DISCUSSION

The first question that we seek to answer is whether the spectral shifts observed in the histograms of Figure 3 are consistent with 6-*s*-*cis* to 6-*s*-*trans* conformational changes of the chromophore. To explore this question, we prepared a set of 10 11-*cis*-retinal Schiff-base chromophores with various covalent substituents that mimic the extremes of electrostatic environments observed within the visual pigments. All but 1 of the 10 models were protonated, and a few involved isolated protonated Schiff bases without counterions. Carboxylate ion groups and perchlorate ions were used to represent negatively charged ions, while iminium ions were introduced to represent positively charged ions near the chromophore. The models are shown in Tables S3 and S4 in the Supporting Information along with the calculated results. The ground-state geometries were minimized using density functional methods [B3LYP/6-31G(d), Gaussian 03, Gaussian Corp., Pittsburgh, PA], and the photophysical properties were calculated using MNDO−PSDCI theory (see the Materials and Methods). The MNDO−PSDCI method has been found to be very reliable for calculating the absorption properties of retinal chromophores, both isolated and protein-bound (*15, 22*). The transition energies into the low-lying strongly allowed excited state are summarized in the histogram of Figure 4. The wavelength shift for our A1 models is comparable to the shift for isolated chromophores observed by Honig and co-workers (*11*). The model chromophore studies predict a 6-*s*-*cis* to 6-*s*-*trans* average bathochromic shift of ∼1680 cm^{-1} for A1 chromophores and ∼1970 cm^{-1} for A2 chromophores (Figure 4), which are to be compared to the observed region 1−3 bathochromic shifts of ∼1500 and ∼2670 cm^{-1}, respectively (Figure 3). The good agreement for the A1 chromophores is encouraging and provides support for our hypothesis. The calculated shift for the A2 chromophores is smaller than the observed shift by roughly 30%. We provide one possible explanation for the larger-than-calculated observed shift based on binding site electrostatics below. Nevertheless, the qualitative agreement is encouraging and provides support for our proposal that the bathochromic shift between regions 1 and 3 is associated with a 6-*s*-*cis* to 6-*s*-*trans* conformational change.

The next step is to explore the energetics of the conformer selection process. The availability of a crystal structure for rhodopsin (*23, 32*) coupled with the significant protein homology within the visual pigment family (*33*) makes homology modeling a viable approach. Our homology modeling methods and procedures are identical to those used previously to study the UV cone pigments (*15*) and include 2 ns molecular dynamics using the Charmm22 force field. The calculations indicate that the pigments that fall under region 3 of our histogram (Figure 3), such as American chameleon red, human red, and canary red, select a 6-*s*-*trans* conformation as shown by lower *s*-*trans* energies (Table 1). This finding supports the hypothesis of Chen and co-workers on iodopsin, a pigment that has an 80% sequence identity

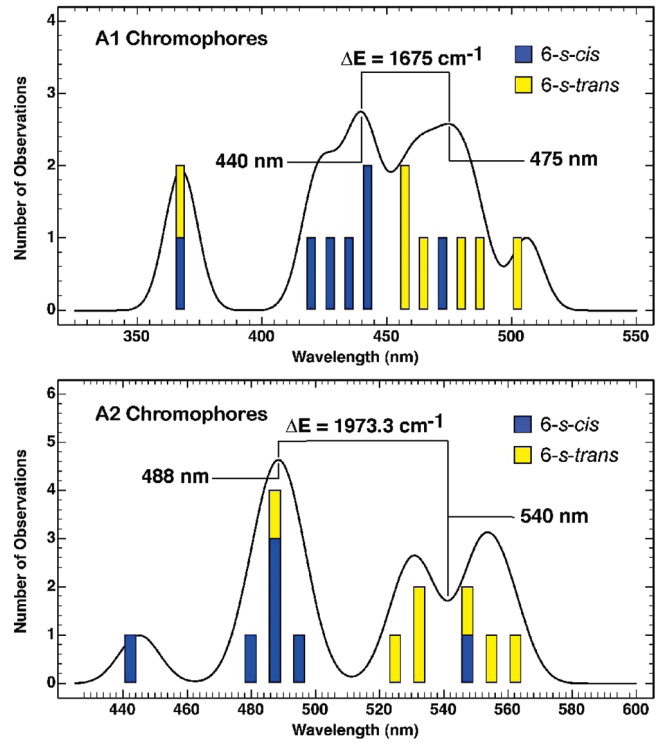

FIGURE 4: Histogram of the transition energies of the 10 model chromophores calculated using the MNDO−PSDCI theory including full single- and double-configuration interaction within the π system. The structures and the data are listed in Tables S3 and S4 in the Supporting Information. The calculations confirm that the 6-*s*-*trans* conformers are on average red-shifted relative to the 6-*s*-*cis* conformers. A histogram analysis reveals that the difference in the transition wavelength between the 6-*s*-*trans* and the 6-*s*-*cis* conformers is similar to that observed between regions 1 and 3 of the experimental A1 and A2 histograms (Figure 3).

Table 1: Comparison of the Calculated Energies of Rhodopsin and Six Cone Pigments Containing 6-*s*-*cis* versus 6-*s*-*trans* Chromophores[a]

	energy (Charmm) (kcal/mol)	
models	6-*s*-*cis*	6-*s*-*trans*
rhodopsin (498 nm)	−7213.735	−7053.548
A1-containing opsins		
dolphin green (524 nm)	−6217.510	−6088.184
human green (531 nm)	−7072.558	−6734.553
human red (560 nm)	−6919.252	−7131.425
canary red (571 nm)	−5127.131	−5159.844
A2-containing opsins		
goldfish green (532 nm)	−6262.406	−6099.316
American chameleon red (625 nm)	−6263.410	−6345.979

[a] Energies following 2 ns molecular dynamics of rhodopsin (1U19)-based homology models (see the text).

with the human red cone opsin. Iodopsin, an A1 region 3 pigment, was proposed by Chen and co-workers to contain a 6-*s*-*trans* ring conformation as part of its spectral tuning mechanism (*17*). The pigments that fall under region 1 of our histogram (dolphin green and goldfish green) gave lower *s*-*cis* energies, indicating that region 1 pigments select a 6-*s*-*cis* ring conformation. However, the energetic difference for the A1 deep red cone is within the error margins of these calculations. The studies on monkey red demonstrate the importance of carrying out long-term (2 ns) molecular dynamics prior to minimization. After 1 ns, the binding site retains a preference for a 6-*s*-*cis* chromophore, and only after 2 ns does the 6-*s*-*trans* chromophore achieve comparative preference. However, a key observation is that these calcula-

Table 2: Comparison of the Calculated Energies of Monkey Red Homology Models Containing 6-*s*-*cis* and 6-*s*-*trans* A1 Retinal Chromophores

models	energy (Charmm) (kcal/mol)	
	6-*s*-*cis*	6-*s*-*trans*
monkey red (560 nm)[a]	−7229.297	−7086.673
monkey red (560 nm)[b]	−6908.607	−7127.620
monkey red (9-*cis*)[b]	−10811.176	−10508.343

[a] The model is based on the human red model that has been run with a 1 ns molecular dynamics. The structure was optimized by ABNR methods, and the energy was calculated (see the text). [b] The same as in [a] but after 2 ns molecular dynamics.

tions do not predict energy differences larger than the intrinsic error in such procedures. Hence, the theoretical results are illustrative but not authoritative.

We also created monkey red models with a 9-*cis* chromophore. Our calculations predict that the monkey red binding site with a 9-*cis* chromophore preferentially selects a 6-*s*-*cis* conformation (Table 2). This result provides insight into the Makino study (*18*), which indicated that the 9-*cis*,6-*s*-*cis* conformer is selected. However, we can find no discrete protein−chromophore interactions that are responsible for selecting 6-*s*-*cis* in the 9-*cis* chromophore but 6-*s*-*trans* in the 11-*cis* chromophore. Rather, we believe this selection process is primarily electrostatic and global to the entire binding site (see the discussion below). Both 9-*cis* and 11-*cis* chromophores are very stable in the binding site, and in the case of monkey red, the 9-*cis* chromophore is calculated to be more stable. This surprising result deserves further study. However, for the purposes of the present study, we conclude that our results and conclusions are consistent with the experimental results reported in Makino et al. (*18*).

Although our calculations on both the A1 and A2 chromophores provide support for the selection of a 6-*s*-*trans* geometry in deep red cone pigments, the evidence is stronger for the A2 pigments for two reasons. The first reason is based on the observation that there are very few pigments found between regions 1 and 3 in the A2 histogram (Figure 3). This observation suggests that a single discrete mechanism is responsible for the spectral shift, and the lack of a residue-based source for this shift suggests that the chromophore may be involved. The 6-*s*-*cis* and 6-*s*-*trans*conformations are separated by a relatively large barrier (>10 kcal/mol in the protein), and hence, these two conformations will not be rapidly interconverting. The protein will then relax to accommodate the conformation to yield a stable absorption band characteristic of the lower energy conformation. This recipe will produce the type of histogram that we observe for the A2 pigments (Figure 3). The second reason that the A2 pigment assignment is more compelling derives from an analysis of the molecular dynamics calculations. During dynamics, the protein equilibrates to provide enhanced stabilization of whatever chromophore is inserted and the 6-*s*-*trans* conformer requires about 400 ps to stabilize in the deep red A2 pigments but often more than 1.6 ns for the deep red A1 pigments. We conclude that ambient temperature differentiation is more efficient in the A2 pigments, and thus, our modeling is more reliable for these pigments. Conversely, the A1 studies are less certain in terms of both

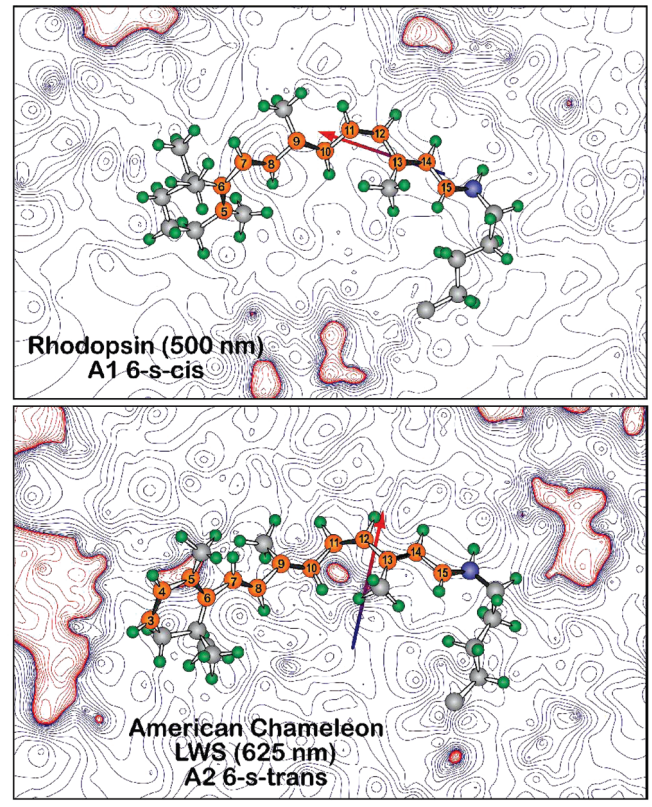

FIGURE 5: Electrostatic contours in the plane of the chromophores of bovine rhodopsin (1U19) and a 6-*s*-*trans* homology model of American chameleon based on 1U19. The contours are based on Mulliken charges from a single SCF PM3 Mozyme calculation on a Charmm-based structure following 2 ns molecular dynamics. The contours are associated with the protein residues, ignoring the chromophore charges. Note that, in both cases, the chromophore is bathed in an electrostatic field that is predominantly negative (blue contours). However, the dipole moment of the binding site is nearly orthogonal between the two proteins, with the rhodopsin binding site favoring a 6-*s*-*cis* conformer (top) and the American chameleon binding site (bottom) favoring a 6-*s*-*trans* conformer.

the histograms (high occupation of region 2) and in the requirement that conformational equilibration requires long-term dynamics.

We cannot identify any discrete protein−chromophore interactions within the binding sites of these proteins that are responsible for preferential selection of the 6-*s*-*trans* conformer. Rather, we conclude that the 6-*s*-*trans* conformer is selected via the combination of two electrostatic effects, which are summarized in Figure 5. This figure compares the electrostatic fields in the plane of the chromophores in rhodopsin (which selects 6-*s*-*cis*) and chameleon red (which selects 6-*s*-*trans*). The atomic charges associated with the positively charged chromophore have been neglected, and hence, the binding site displays a net negative charge. In the case of rhodopsin, a majority of the negative charge is concentrated near the protonated Schiff base. In contrast, the negative charge in chameleon red is more evenly distributed, which means that there is a net shift of negative charge toward the ring. An examination of Figure 2 provides a good perspective on why this result will enhance stabilization of the 6-*s*-*trans* conformation, which has a charge distribution that shifts more chromophore positive charge toward the ring. Dipole–

dipole interactions are also important. In American chameleon red, the net dipole moment of the binding site is oriented orthogonal to the chromophore, whereas in rhodopsin, the dipole moment of the binding site is along the axis of the chromophore. The former situation preferentially stabilizes the 6-*s*-*trans* conformer, and the latter preferentially stabilizes the 6-*s*-*cis* conformer. We refer to the above effects as electrostatic steering and note that an increasing negative charge near the ring will also enhance the red shift associated with the low-lying strongly allowed $^1B_u^+$-like state. This follows from the fact that, upon excitation, negative charge is shifted toward the Schiff base. This charge shift will enhance the stability of the excited state relative to the ground state when the negative charge is shifted toward the ring. This observation may explain why the region 1−3 separation is about 30% larger for the A2 pigments than that calculated on the basis of the isolated models.

What remains to be explained is what conformation is selected in those A1 pigments that occupy region 2 of Figure 3. We do not have an answer to this question. Homology calculations on two pigments in this region were ambiguous, and it is possible that a mixture of 6-*s*-*cis* and 6-*s*-*trans* conformers are present in some of these pigments.

SUPPORTING INFORMATION AVAILABLE

Over 200 absorption maxima of various vertebrate red cone pigments used to generate the histograms shown in Figure 3, as well as a summary of the quantum mechanical calculations. This information is available free of charge via the Internet at http://pubs.acs.org.

REFERENCES

1. Ebrey, T., and Koutalos, Y. (2001) Vertebrate photoreceptors. *Prog. Retinal Eye Res. 20*, 49–94.
2. Yokoyama, S., and Radlwimmer, F. B. (2001) The molecular genetics and evolution of red and green color vision in vertebrates. *Genetics 158*, 1697–1710.
3. Dartnall, H. J., and Lythgoe, J. N. (1965) The spectral clustering of visual pigments. *Vision Res. 5*, 81–100.
4. Harosi, F. I. (1994) An analysis of two spectral properties of vertebrate visual pigments. *Vision Res. 34*, 1359–1367.
5. Reckel, F., Melzer, R. R., Parry, J. W. L., and Bowmaker, J. K. (2002) The retina of five atherinomorph teleosts: Photoreceptors, patterns and spectral sensitivities. *Brain, Behav., Evol. 60*, 249–264.
6. Provencio, I., Loew, E. R., and Foster, R. G. (1992) Vitamin A2-based visual pigments in fully terrestrial vertebrates. *Vision Res. 32*, 2201–2208.
7. Nakanishi, K., Balogh-Nair, V., Arnaboldi, M., Tsujimoto, K., and Honig, R. (1980) An external point-charge model for bacteriorhodopsin to account for its purple color. *J. Am. Chem. Soc. 102*, 7945–7947.
8. Kropf, A., and Hubbard, R. (1958) The mechanism of bleaching rhodopsin. *Ann. N.Y. Acad. Sci. 74*, 266–280.
9. Oseroff, A. R., and Callender, R. H. (1974) Resonance Raman spectroscopy of rhodopsin in retinal disk membranes. *Biochemistry 13*, 2443–2348.
10. Mathies, R., Freedman, T. B., and Stryer, L. (1977) Resonance Raman studies of the conformation of retinal in rhodopsin and isorhodopsin. *J. Mol. Biol. 109*, 367–372.
11. Honig, B., Greenberg, A. D., Dinur, U., and Ebrey, T. G. (1976) Visual-pigment spectra: Implications of the protonation of the retinal Schiff base. *Biochemistry 15*, 4593–4599.
12. Yoshizawa, T. (1992) The road to color vision: Structure, evolution and function of chicken and gecko visual pigments. *Photochem. Photobiol. 56*, 859–867.
13. Lin, S. W., Kochendoerfer, G. G., Carroll, K. S., Wang, D., Mathies, R. A., and Sakmar, T. P. (1998) Mechanisms of spectral tuning in blue cone visual pigments: Visible and Raman spectroscopy of blue-shifted rhodopsin mutants. *J. Biol. Chem. 273*, 24583–24591.
14. Vought, B. W., Dukkipatti, A., Max, M., Knox, B. E., and Birge, R. R. (1999) Photochemistry of the primary event in short-wavelength visual opsins at low temperature. *Biochemistry 38*, 11287–11297.
15. Kusnetzow, A. K., Dukkipati, A., Babu, K. R., Ramos, L., Knox, B. E., and Birge, R. R. (2004) Vertebrate ultraviolet visual pigments: Protonation of the retinylidene Schiff base and a counterion switch during photoactivation. *Proc. Natl. Acad. Sci. U.S.A. 101*, 941–946.
16. Fasick, J. I., Applebury, M. L., and Oprian, D. D. (2002) Spectral tuning in the mammalian short-wavelength sensitive cone pigments. *Biochemistry 41*, 6860–6865.
17. Chen, J. G., Nakamura, T., Ebrey, T. G., Ok, H., Konno, K., Derguini, F., Nakanishi, K., and Honig, B. (1989) Wavelength regulation in iodopsin, a cone pigment. *Biophys. J. 55*, 725–729.
18. Makino, C. L., Kraft, T. W., Mathies, R. A., Lugtenburg, J., Miley, M. E., van der Steen, R., and Baylor, D. A. (1990) Effects of modified chromophores on the specral sensitivity of salamander, squirrel and macaque cones. *J. Physiol. 424*, 545–560.
19. Frisch, M. J., Trucks, G. W., Schlegel, H. B., Scuseria, G. E., Robb, M., Cheeseman, J. R., Jr., Vreven, T., Kudin, K. N., Burant, J. C., Millam, J. M., Iyengar, S. S., Tomasi, J., Barone, V., Mennucci, B., Cossi, M., Scalmani, G., Rega, N., Petersson, G. A., Nakatsuji, H., Hada, M., Ehara, M., Toyota, K., Fukuda, R., Hasegawa, J., Ishida, M., Nakajima, T., Honda, Y., Kitao, O., Nakai, H., Klene, M., Li, X., Knox, J. E., Hratchian, H. P., Cross, J. B., Adamo, C., Jaramillo, J., Gomperts, R., Stratmann, R. E., Yazyev, O., Austin, A. J., Cammi, R., Pomelli, C., Ochterski, J., Ayala, P. Y., Morokuma, K., Voth, G. A., Salvador, P., Dannenberg, J. J., Zakrzewski, V. G., Dapprich, S., Daniels, A. D., Strain, M. C., Farkas, O., Malick, D. K., Rabuck, A. D., Raghavachari, K., Foresman, J. B., Ortiz, J. V., Cui, Q., Baboul, A. G., Clifford, S., Cioslowski, J., Stefanov, B. B., Liu, G., Liashenko, A., Piskorz, P., Komaromi, I., Martin, R. L., Fox, D. J., Keith, T. A., Al-Laham, M. A., Peng, C. Y., Nanayakkara, A., Challacombe, M., Gill, P. M. W., Johnson, B., Chen, W., Wong, M. W., Gonzalez, C., and Pople, J. A. (2003) Gaussian 03, Gaussian, Inc., Wallingford, CT.
20. Shima, S., Ilagan, R. P., Gillespie, N., Sommer, B. J., Hiller, R. G., Sharples, F. P., Frank, H. A., and Birge, R. R. (2003) Two-photon and fluorescence spectroscopy and the effect of environment on the photochemical properties of peridinin in solution and in the peridinin−chlorophyll−protein from *Amphidinium carterae*. *J. Phys. Chem. A 107*, 8052–8066.
21. Martin, C. H., and Birge, R. R. (1998) Reparameterizing MNDO for excited state calculations using ab initio effective Hamiltonian theory: Application to the 2,4-pentadien-1-iminium cation. *J. Phys. Chem. A 102*, 852–860.
22. Ren, L., Martin, C. H., Wise, K. J., Gillespie, N. B., Luecke, H., Lanyi, J. K., Spudich, J. L., and Birge, R. R. (2001) Molecular mechanism of spectral tuning in sensory rhodopsin II. *Biochemistry 40*, 13906–13914.
23. Okada, T., Sugihara, M., Bondar, A.-N., Elstner, M., Entel, P., and Buss, V. (2004) The retinal conformation and its environment in rhodopsin in light of a new 2.2 Å crystal structure. *J. Mol. Biol. 342*, 571–583.
24. Allinger, N. L., and Burkert, U. (1982) *Molecular Mechanics*, American Chemical Society, Washington, D.C.
25. Allinger, N. L., Kuang, J., and Thomas, H. D. (1990) Molecular mechanics (MM2 and MM3) calculations on aliphatic and aromatic nitro compounds. *THEOCHEM 68*, 125–148.
26. Brooks, B., Bruccoleri, R. E., Olafson, B. D., States, D. J., Swaminathan, S., and Karplus, M. (1983) CHARMM: A program for macromolecular energy, minimization, and dynamics calculations. *J. Comput. Chem. 4*, 187–217.
27. MacKerell, A. D., Jr., Bashford, D., Bellott, M., Dunbrack, R. L., Jr., Evanseck, J. D., Field, M. J., Fischer, S., Gao, J., Guo, H., and Ha, S. (1998) All-atom empirical potential for molecular modeling and dynamics studies of proteins. *J. Phys. Chem. B 102*, 3586–3616.
28. Hermone, A., and Kuczera, K. (1998) Free-energy simulations of the retinal cis−trans isomerization in bacteriorhodopsin. *Biochemistry 37*, 2843–2853.
29. Lin, S. W., Imamoto, Y., Fukada, Y., Shichida, Y., Yoshizawa, T., and Mathies, R. A. (1994) What makes red visual pigments

red? A resonance Raman microprobe study of retinal chromophore structure in iodopsin. *Biochemistry 33*, 2151–2160.

30. Neitz, M., Neitz, J., and Jacobs, G. H. (1991) Spectral tuning of pigments underlying red−green color vision. *Science 252*, 971–974.
31. Chan, T., Lee, M., and Sakmar, T. P. (1992) Introduction of hydroxyl-bearing amino acids causes bathochromic spectral shifts in rhodopsin. Amino acid substitutions responsible for red−green color pigment spectral tuning. *J. Biol. Chem. 267*, 9478–9480.
32. Palczewski, K., Kumasaka, T., Hori, T., Behnke, C. A., Motoshima, H., Fox, B. A., Le Trong, I., Teller, D. C., Okada, T., Stenkamp, R. E., Yamamoto, M., and Miyano, M. (2000) Crystal structure of rhodopsin: A G protein-coupled receptor. *Science 289*, 739–745.
33. Nathans, J., Thomas, D., and Hogness, D. S. (1986) Molecular genetics of human color vision: The genes encoding blue, green and red pigments. *Science 232*, 193–202.

BI702069D

Supporting Information for

"Spectral Tuning of Deep Red Cone Pigments"

Tabitha L. Amora, Lavoisier S. Ramos, Jhenny F. Galan and Robert R. Birge

This section provides the literature sources for the absorption maxima of the A1 and A2 vertebrate M/LWS pigments as well as additional details regarding the theoretical methods. Our principal conclusion is that the deep red pigments achieve an enhanced bathochromic shift by selecting a 6-*s*-*trans* conformation of the bound chromophore. Those pigments which are predicted to adopt a 6-*s*-*trans* A2 chromophore are indicated in solid rectangles. We consider these assignments compelling. Those pigments which are predicted to adopt a 6-*s*-*trans* A1 chromophore are indicated in dashed rectangles. We consider these assignments tentative. All the other pigments shown have 6-*s*-*cis* A1 or A2 chromophores.

Over 200 absorption maxima of vertebrate M/LWS pigments from various literature sources are collected in Tables S1 (A1 chromophores) and S2 (A2 chromophores). These data were used to generate the histograms shown in Figure 3.

The isolated chromophore models that we used to examine the effect of 6-*s*-*cis* versus 6-*s*-*trans* conformation on the electronic properties of the isolated chromophores are shown in Tables S3 and S4. The ground state geometries of the models were minimized by DFT methods in Gaussian-03 (*29*). The B3LYP/6-31G(d) Hamiltonian was selected. The excited state properties were calculated by using MNDO-PSDCI theory (*30*-*33*). The molecular diagram that is shown to the left of the data shows the geometry of the chromophore with the lowest energy conformation. In general, protonated Schiff bases without counterions select the 6-*s*-*trans*. Most others select 6-*s*-*cis*.

Table S1: The absorption maxima of various A1-containing vertebrates collected from literature data. These data were used to generate the histograms in Figure 3.

λ_{max}	**Origin of A1 Pigment**	**Reference**
440	European ground squirrel *(Citellus citellus)*	(*34*)
502	Frog *(Xenopus laevis)*	(*35*)
503	Blue tit *(Parus caeruleus)*	(*36*)
505	Rudd (summer) *(Scardinius erythrophthalmus)*	(*37*)
508	Mouse	(*38*)
510	Mouse	(*39*)
511.6	*Batrachocottus nicolski* (300-1000 m)	(*40*)
512	Wolf-eel *(Anarrhichthys ocellatus)*	(*41*)
512.3	*Limnocottus eurystomus* (100-500 m)	(*40*)
512.6	*Asprocottus intermedius* (100-500 m)	(*40*)
513	Dwarf wrymouth *(Lyconectes aleutensis)*	(*41*)
513	English sole *(Parophrys vetula)*	(*41*)
513	Great sculpin *(Myoxocephalus polyacanthocephalus)*	(*41*)
513	Grunt sculfin *(Rhamphocottus richardsoni)*	(*41*)
513	Lingcod *(Ophiodon elongatus)*	(*41*)
513	Rock prickleback *(Xiphister mucosus)*	(*41*)
514	Pacific sandfish *(Trichodon trichodon)*	(*41*)
516	Coral fish *(Dascyllus trimaculatus)*	(*42*)
516	Guinea pig *(Cavia porcellus)*	(*43*)
516	Kelp greenling *(Hexagrammos decagrammus)*	(*41*)
516	Pudget sound sculpin *(Artidius meanyi)*	(*41*)
517	Guillfish *(Ptilichthys goodei)*	(*41*)
517.3	*Batrachocottus multiradiatus* (100-500 m)	(*40*)
519	Great sculpin *(Myoxocephalus polyacanthocephalus)*	(*41*)
519	Pudget sound sculpin *(Artidius meanyi)*	(*41*)
519	White-spotted greenling *(Hexagrammos stelleri)*	(*41*)
519	Young larval flounder	(*44*)
520	Brown rockfish *(Sebastes auricaulatus)*	(*41*)
520	Walleye pollock *(Theragra chalcogramma)*	(*41*)
520	White-spotted greenling *(Hexagrammos stelleri)*	(*41*)
520.6	*Cottocomephorus inermis* (50-450 m)	(*40*)
521	Brown rockfish *(Sebastes auricaulatus)*	(*41*)
521	*Batrachocottus baicalensis* (1-120 m)	(*40*)
521	House gecko *(Hemidactylus garnotii)*	(*45*)
521	Pacific herring *(Clupea pallasi)*	(*41*)
521	Tokay Gecko *(Gecko gecko)*	(*46*)
521.2	*Paracottus kneri* (2-5 m)	(*40*)

Table S1 continued

522	Pacific herring *(Clupea pallasi)*	(*41*)
522	West Australian dhufish *(Glaucosoma hebraicum)*	(*47*)
522	White-spotted greenling *(Hexagrammos stelleri)*	(*41*)
522.6	*Paracottus kneri* (2-5 m)	(*40*)
523.3	*Cottocomephorus grewingki* (1-300 m)	(*40*)
524	Dolphin (bottlenose) *(Tursiops truncatus)*	(*48*)
524	Kelp greenling *(Hexagrammos decagrammus)*	(*41*)
525	Baikal Cottoids-shallow water	(*40*)
525	*Cottus kessleri* (2-5 m)	(*40*)
525	Hawaiin saddle wrasse *(Thalassoma duperrey)*	(*49*)
526	Mediterranean gecko *(Hemidactylus turcicus)*	(*45*)
526	Pink surfperch *(Zalembius rosaceus)*	(*50*)
527	Pacific sand lance *(Ammodytes hexapterus)*	(*41*)
528	Weever fish *(Trachinus vipera)*	(*51*)
529	Northern anchovy *(Engraulis mordax)*	(*41*)
529	Shiner surfperch *(Cymatogaster aggregata)*	(*50*)
530	Cave fish *(Astyanax fasciatus)*	(*52*)
530	Chimpanzee *(Pan troglodytes)*	(*53*)
530	Guinea pig *(Cavia porcellus)*	(*54*)
530	Human *(Homo sapiens)*	(*55*)
530	Northern anchovy *(Engraulis mordax)*	(*41*)
530	Tammar wallaby *(Macropus eugenii)*	(*56*)
530.7	Diana monkey *(Cercopithecus diana)*	(*57*)
531	Deer *(Odocoileus virginianus)*	(*43*)
531	Rainbow trout *(Oncorhynchus mykiss)*	(*58*)
531	Winter adult flounder *(Pseudopleuronectes americanus)*	(*44*)
532	American/squirrel monkey *(Saimuri sciureus)*	(*59*)
532	Coral fish *(Pomacentrus coelestis)*	(*60*)
532	Squirrel *(Sciurius carolinensis)*	(*43*)
533	Guppy *(Poecilia reticulata)*	(*61*)
533	Malawi cichlid fish *(Metriaclima zebra)*	(*62*)
533	Moustached guenon *(Cercopithecus cephus)*	(*57*)
533	Patas monkey *(Erythrocebus patas)*	(*57*)
533	Scinc gecko *(Teratoscincus scincus)*	(*45*)
533.3	*Cercopithecus talapoin*	(*57*)
533.9	Spot-nosed monkey *(Cercopithecus petaurista)*	(*57*)
534	Blind mole rat *(Spalax ehrenbergi)*	(*63*)
535	Black bream *(Acanthopagrus butcheri)*-young	(*64*)
535	Fat-tailed dunnart *(Sminthopsis crassicaudata)*	(*65*)
535	Grivet *(Cercopithecus aethiops)*	(*57*)
535.2	*Papio papio* (ii)	(*57*)

Table S1 continued

535.6	*Papio papio* (iv)	(*57*)
536	American/squirrel monkey *(Saimuri sciureus)*	(*66*)
536	*Dimidiochromis compressiceps*	(*62*)
536	Epigean fish *(Astyanax fasciatus)*	(*67*)
536	Rhesus macaque *(Macaca mulatta)*	(*57*)
536.4	*Papio papio* (i)	(*57*)
537	White-tailed deer *(Odocoileus virginiana)*	(*68*)
538.8	*Papio papio* (iii)	(*57*)
539	Horse *(Equus caballus)*	(*69*)
539	Marmoset (New world monkey) *(Callithrix jacchus)*	(*43*)
540	Ring-tailed lemur *(Lemur catta)*	(*70*)
541	Kelp greenling *(Hexagrammos decagrammus)*	(*41*)
541	Saddle-backed tamarin *(Saguinus fuscicollis)*	(*59*)
42	Fallow deer *(Dama dama)*	(*68*)
543	Owl monkey *(Aotus trivirgatus)*	(*71*)
543	Penguin *(Spheniscus humboldti)*	(*36*)
544	Golden lion tamarin *(Leontopithecus rosalia rosalia)*	(*72*)
545	Black bream *(Acanthopagrus butcheri)*-adult	(*64*)
545	Golden-handed tamarin *(Saguinus midis)*	(*72*)
545	Horse *(Equus caballus)*	(*43*)
545	Saddle-backed tamarin *(Saguinus fuscicollis)*	(*73*)
546	Cotton top tamarin *(Saguinus oedipus)*	(*72*)
546	*Cottus kessleri* (2-5 m)	(*40*)
547	American/squirrel monkey *(Saimuri Sciureus)*	(*59*)
547	Ring-tailed lemur *(Lemur catta)*	(*72*)
547	Winter adult flounder *(Pseudopleuronectes americanus)*	(*44*)
548.3	Zebrafish *(Danio rerio)*	(*74*)
549	American/squirrel monkey *(Saimuri sciureus)*	(*66*)
549	Boa constrictor imperator	(*75*)
549	Dusky titi *(Callicebus moloch)*	(*73*)
551	Ball python *(Python regius)*	(*76*)
552	Sheep *(Ovis aries)*	(*68*)
553	Cat *(Felis catus)*	(*43*)
553	Goat *(Capra hircus)*	(*68*)
553	Marmoset (New world monkey) *(Callithrix jacchus)*	(*43*)
554	Garter Snake *(Thamnophis sirtalis)*	(*76*)
554	Golden lion tamarin *(Leontopithecus rosalia rosalia)*	(*72*)
554	White-spotted greenling *(Hexagrammos stelleri)*	(*41*)
555	Arctic fox *(Alopex lagopus)*	(*71*)

Table S1 continued

555	Cow/Bovine *(Bos taurus)*	(*68*)
555	Domestic dog *(Canis familiaris)*	(*71*)
555	Island gray foxes *(Urocyon littoralis)*	(*71*)
555	Lamprey	(*35*)
555	Red foxes *(Vulpes vulpes)*	(*71*)
555	Tawny Owl *(Strix aluco)*	(*36*)
555	Tree Shew *(Tupaia belangeri)*	(*77*)
556	Blackbird *(Turdus merula)*	(*78*)
556	Saddle-backed tamarin *(Saguinus fuscicollis)*	(*59*)
557	Blackbird *(Turdus merula)*	(*36*)
557	Cotton top tamarin *(Saguinus oedipus)*	(*72*)
557	Frog *(Xenopus laevis)*	(*52*)
557	Golden-handed tamarin *(Saguinus midis)*	(*72*)
557	Honey possum *(Tarsipes rostratus)*	(*65*)
557	Pig *(Sus scrofa)*	(*68*)
557	Saddle-backed tamarin *(Saguinus fuscicollis)*	(*73*)
557.7	Zebrafish *(Danio rerio)*	(*74*)
558	Cave fish *(Astyanax fasciatus)*	(*52*)
558	White-spotted greenling *(Hexagrammos stelleri)*	(*41*)
560	American chameleon (regenerated)	(*79*)
560	Chameleon *(Anolis)*	(*79*)
560	Chimpanzee *(Pan troglodytes)*	(*53*)
560	Cyprinid fish *(Danio aequipinnatus)*	(*80*)
560	Human *(Homo sapiens)*	(*81*)
560	Laughing gull *(Larus atricilla)*	(*36*)
560	Zebrafinch *(Taeniopygia guttata)*	(*81*)
561	American/squirrel monkey *(Saimuri sciureus)*	(*59*)
561	Chameleon *(Anolis)*	(*52*)
561	Dusky titi *(Callicebus moloch)*	(*73*)
561	Marmoset (New world monkey) *(Callithrix jacchus)*	(*43*)
561.5	Rhesus macaque *(Macaca mulatta)*	(*57*)
562	Lingcod *(Ophiodon elongatus)*	(*41*)
562	Saddle-backed tamarin *(Saguinus fuscicollis)*	(*73*)
562	White-headed munia *(Louchura maja)*	(*36*)
562.7	Spot-nosed monkey *(Cercopithecus petaurista)*	(*57*)
563	Blue tit *(Parus caeruleus)*	(*36*)
563	Cotton top tamarin *(Saguinus oedipus)*	(*72*)
563	Cut-throat finches *(Amadina fasciata)*	(*36*)
563	European Starling *(Sturnus vulgaris)*	(*36*)
563	Gouldian finch *(Erythrura gouldiae)*	(*36*)
563	House sparrow (Passer domesticus)	(*36*)
563	Mummichog killifish *(Fundulus heteroclitus)*	(*82*)

Table S1 continued

563	Plum-headed finch *(Neochmia modesta)*	(*83*)
563	Saddle-backed tamarin *(Saguinus fuscicollis)*	(*72*)
563	Turkey *(Meleagris galoparco)*	(*36*)
563	White-headed munia *(Louchura maja)*	(*83*)
564	American/squirrel monkey *(Saimuri sciureus)*	(*66*)
564	Brushland tinamou *(Nothoprocta cinerascens cinerascens)*	(*36*)
564	Budgerigar (parakeet) *(Melosittacus undulatus)*	(*36*)
564	*Cercopithecus talapoin*	(*57*)
564	Cut-throat finches *(Amadina fasciata)*	(*83*)
564	Gouldian finch *(Erythrura gouldiae)*	(*83*)
564	Plum-headed finch *(Neochmia modesta)*	(*83*)
564	White-headed munia *(Louchura maja)*	(*83*)
564	Zebrafish *(Danio rerio)*	(*84*)
564.3	*Papio papio* (i)	(*57*)
564.4	*Papio papio* (iii)	(*57*)
565	Blue tit *(Parus caeruleus)*	(*78*)
565	Gouldian finch *(Erythrura gouldiae)*	(*83*)
565	Plum-headed finch *(Neochmia modesta)*	(*36*)
565	Rook *(Corvus frugilegus)*	(*36*)
565	Rudd (summer) *(Scardinius erythrophthalmus)*	(*37*)
565.3	Moustached guenon *(Cercopithecus cephus)*	(*57*)
565.7	*Papio papio* (ii)	(*57*)
565.9	Diana monkey *(Cercopithecus diana)*	(*57*)
566	Chilean tinamou *(Nothoprocta perdicaria sanborni)*	(*36*)
566	Epigean fish *(Astyanax fasciatus)*	(*67*)
566	Peacock /Peafowl *(Pavo cristatus)*	(*36*)
566.3	Grivet *(Cercopithecus aethiops)*	(*57*)
566.3	Patas monkey *(Erythrocebus patas)*	(*57*)
567	Emu *(Dromiceius novae-hollandiae)*	(*36*)
567	Japanese quail *(Coturnix japonica)*	(*36*)
567	Mallard duck *(Anas platyrhynchos)*	(*36*)
567	Pacific sandfish *(Trichodon trichodon)*	(*41*)
567	Pekin robin *(Lotothrix lutea)*	(*36*)
567	Rock dove (Feral pigeon) *(Columba livia)*	(*36*)
567	Zebrafinch *(Taeniopygia guttata)*	(*36*)
567.8	*Papio papio* (iv)	(*57*)
568	Red Irish lord *(Hemilepidotus hemilepidotus)*	(*41*)
569	Cabezon *(Scorpaenichthys marmoratus)*	(*41*)
569	*Dimidiochromis compressiceps*	(*62*)
570	Aylesbury duck *(Anas playrhynchos domesticus)*	(*36*)
570	Chicken *(Gallus gallus)*	(*36*)

Table S1 continued

570	Hawaiin saddle wrasse *(Thalassoma duperrey)*	(*49*)
570	Khaki Campbell duck (*Anas playrhynchos domesticus)*	(*36*)
570	Ostrich *(Strutio camelus)*	(*36*)
570	Rhea *(Rhea americana)*	(*36*)
571	Canary *(Serinus canaria)*	(*36*)
571	Ornate dragon lizards *(Ctenophorus ornatus)*	(*85*)
572	Giant danio *(Danio malabaricus)*	(*42*)
572	Guppy *(Poecilia reticulata)*	(*61*)
574	Dwarf wrymouth *(Lyconectes aleutensis)*	(*41*)
574	Rainbow trout *(Oncorhynchus mykiss)*	(*58*)
575	Black bream *(Acanthopagrus butcheri)*-adult	(*64*)
575	Frog *(Xenopus laevis)*	(*35*)
575	Laughing gull *(Larus atricilla)*	(*36*)
575	Salamander	(*86*)
582	Saddle-backed tamarin *(Saguinus fuscicollis)*	(*59*)
584	Pacific herring *(Clupea pallasi)*	(*41*)

Table S2: The absorption maxima of various A2-containing vertebrate visual pigments. These data were used to generate Figure 3.

λ_{max}	**Origin of A2 Pigment**	**Reference**
515	Red-eared turtle *(Trachemys scripta)*	(*87*)
515	Rudd (winter) *(Scardinius erythrophthalmus)*	(*37*)
515	Southern hemisphere lamprey *(Geotria australis)*	(*88*)
521	Shovelnose sturgeon *(Scaphirhynchus platorynchus)*	(*89*)
525	Sea lamprey (upstream migrant) *(Petromyzon marinus)*	(*90*)
527	Frog *(Xenopus laevis)*	(*35*)
530	Freshwater turtle	(*87*)
531	Kelp surfperch *(Brachyistius frenatus)*	(*50*)
531	Kissing gourami *(Helostoma temminckii)*	(*91*)
531	Rainbow surfperch *(Hypsurus caryi)*	(*50*)
532	Adult green sunfish (native retina)	(*92*)
532	Goldfish *(Carassius auratus)*	(*42*)
534	Adult green sunfish (regenerated retina)	(*92*)
534	Black surfperch *(Embiotoca jacksoni)*	(*50*)
535	Adult european perch *(Perca fluviatilis)*	(*93*)
535	Brown trout *(Salmo trutta)*	(*94*)
535	Paddlefish *(Polyodon spathula)*	(*89*)
536	Striped surfperch *(E. lateralis)*	(*50*)
538	Carp *(Cyprinus carpio)*	(*95*)
538	Reef surfperch *(Micrometrus aurora)*	(*50*)
539	White sturgeon *(Acipenser transmontanus)*	(*96*)
542	Striped bass *(Morone saxatilis)*	(*97*)
542	Sturgeon (boneless fish w/jaws) *(Acipenser stellatus)*	(*98*)
544	Pile surfperch *(Damalichthys vacca)*	(*50*)
545	Dwarf surfperch *(M. minimus)*	(*50*)
545	Siberian sturgeon *(Acipenser baeri)*	(*99*)
559	Goldfish *(Carassius auratus)*	(*81*)
560	Adult yellow perch *(Perca flavescens)*	(*100*)
567	Epigean fish *(Astyanax fasciatus)*	(*67*)
600	Brown trout *(Salmo trutta)*	(*94*)
600	Sea lamprey (upstream migrant) *(Petromyzon marinus)*	(*90*)
602	Silver dollar *(Metynnis argenteus)*	(*91*)
605	Striped bass *(Morone saxatilis)*	(*97*)
605	White sturgeon *(Acipenser transmontanus)*	(*96*)
607	Paddlefish *(Polyodon spathula)*	(*89*)
610	Rudd (winter) *(Scardinius erythrophthalmus)*	(*37*)

Table S2 continued

610	Shovelnose sturgeon *(Scaphirhynchus platorynchus)*	(*89*)
610	Southern hemisphere lamprey *(Geotria australis)*	(*88*)
611	Epigean fish *(Astyanax fasciatus)*	(*67*)
611	Tiger salamander *(Ambystoma tigrinum)*	(*91*)
613	Siberian sturgeon *(Acipenser baeri)*	(*99*)
613	Sturgeon (boneless fish w/jaws) *(Acipenser stellatus)*	(*98*)
614	Goldfish (*Carassius auratus)*	(*57*)
616	Southern hemisphere lamprey *(Geotria australis)*	(*88*)
617	Red-eared turtle *(Trachemys scripta)*	(*87*)
618	Adult green sunfish (regenerated retina)	(*92*)
619	Carp *(Cyprinus carpio)*	(*95*)
620	Adult european perch *(Perca fluviatilis)*	(*93*)
620	Adult green sunfish (native retina)	(*92*)
620	Adult yellow perch *(Perca flavescens)*	(*100*)
620	Freshwater turtle	(*87*)
620	Frog *(Xenopus laevis)*	(*35*)
620	Goldfish *(Carassius auratus)*	(*42*)
620	Salamander	(*86*)
622	Adult green sunfish (regenerated retina)	(*92*)
623	Adult green sunfish (regenerated retina)	(*92*)
623	Rainbow trout *(Oncorhynchus mykiss)*	(*58*)
625	American chameleon *(Anolis carolinensis)*	(*79*)
628	Silver dollar *(Metynnis argenteus)*	(*91*)
630	Kissing gourami *(Helostoma temminckii)*	(*91*)

Table S3: A1 chromophore models and the calculated properties.

A1-methyl	Property	6-s-cis	6-s-trans
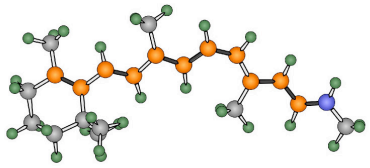	E_0 (Hartree)	-874.0099487	-874.0106355
	ΔE_0 (kJ/mol)		-1.8033
	μ (Debye)	14.7942 D	12.2555 D
	$\Delta E_1[^1B_u^+]$ (eV)	1.794	1.651
	$\Delta\Delta E_1(cm^{-1})$	1153.37	

A1-ethyl syn	Property	6-s-cis	6-s-trans
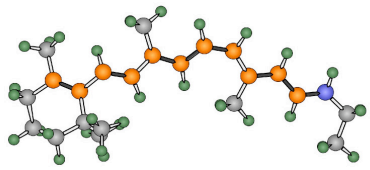	E_0 (Hartree)	-913.3258308	-913.3263636
	ΔE_0 (kJ/mol)		-1.3987
	μ (Debye)	13.9217 D	11.444 D
	$\Delta E_1[^1B_u^+]$ (eV)	1.859	1.702
	$\Delta\Delta E_1(cm^{-1})$	1266.29	

A1-methyl PSB with water	Property	6-s-cis	6-s-trans
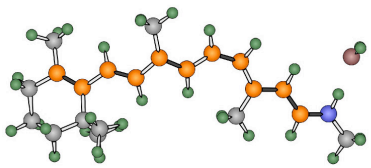	E_0 (Hartree)	-950.4403733	-950.4406926
	ΔE_0 (kJ/mol)		-0.8381
	μ (Debye)	17.1663 D	14.8810 D
	$\Delta E_1[^1B_u^+]$ (eV)	1.944	1.778
	$\Delta\Delta E_1(cm^{-1})$	1338.88	

A1-asp up	Property	6-s-cis	6-s-trans
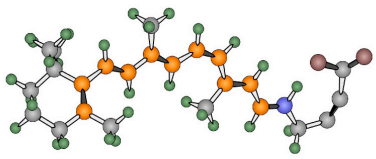	E_0 (Hartree)	-1138.2519527	-1138.2508251
	ΔE_0 (kJ/mol)	-2.9595	
	μ (Debye)	19.3888 D	20.9135 D
	$\Delta E_1[^1B_u^+]$ (eV)	2.916	2.686
	$\Delta\Delta E_1(cm^{-1})$	1855.07	

A1-asp down with water	Property	6-s-cis	6-s-trans
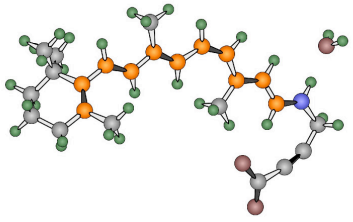	E_0 (Hartree)	-1214.6844769	-1214.6831974
	ΔE_0 (kJ/mol)	-3.3594	
	μ (Debye)	17.7658 D	18.4510 D
	$\Delta E_1[^1B_u^+]$ (eV)	2.803	2.652
	$\Delta\Delta E_1(cm^{-1})$	1217.90	

Table S3 continued

A1-asp up with water	Property	6-s-cis	6-s-trans
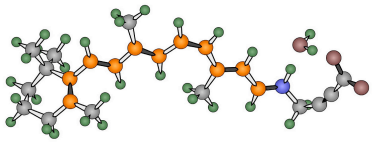	E_0 (Hartree)	-1214.7008698	-1214.6998068
	ΔE_0 (kJ/mol)	-2.7908	
	μ (Debye)	21.9301 D	23.4727 D
	$\Delta E_1[^1B_u^+]$ (eV)	2.856	2.587
	$\Delta\Delta E_1(cm^{-1})$	2169.63	

A1-perchlorate	Property	6-s-cis	6-s-trans
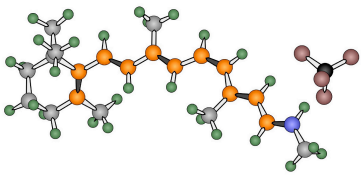	E_0 (Hartree)	-1634.9331931	-1634.9316832
	ΔE_0 (kJ/mol)	-3.9642	
	μ (Debye)	16.3589 D	17.1504 D
	$\Delta E_1[^1B_u^+]$ (eV)	2.808	2.547
	$\Delta\Delta E_1(cm^{-1})$	2105.11	

A1-9-NH_2 asp up	Property	6-s-cis	6-s-trans
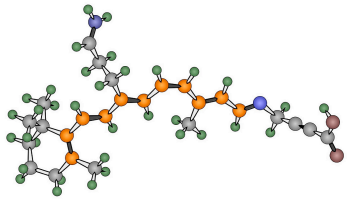	E_0 (Hartree)	-1271.4094225	-1271.4085495
	ΔE_0 (kJ/mol)	-2.2919	
	μ (Debye)	25.2682 D	26.8006 D
	$\Delta E_1[^1B_u^+]$ (eV)	3.380	3.352
	$\Delta\Delta E_1(cm^{-1})$	225.84	

A1-perchlorate with 2 waters	Property	6-s-cis	6-s-trans
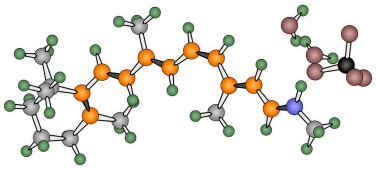	E_0 (Hartree)	-1787.8018522	-1787.8002316
	ΔE_0 (kJ/mol)	-4.2549	
	μ (Debye)	15.7714 D	16.8875 D
	$\Delta E_1[^1B_u^+]$ (eV)	2.947	2.727
	$\Delta\Delta E_1(cm^{-1})$	1774.42	

A1-9-glu asp up	Property	6-s-cis	6-s-trans
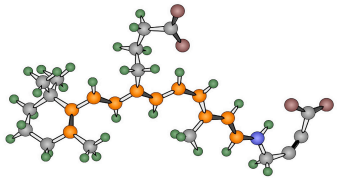	E_0 (Hartree)	-1404.9008078	-1404.89898404
	ΔE_0 (kJ/mol)	-4.7882	
	μ (Debye)	31.3423 D	32.2276 D
	$\Delta E_1[^1B_u^+]$ (eV)	2.613	2.450
	$\Delta\Delta E_1(cm^{-1})$	1314.68	

Table S4: A2 chromophore models and the calculated properties.

A2-methyl	Property	6-s-cis	6-s-trans
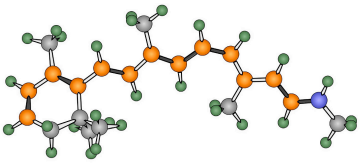	E_0 (Hartree)	-872.7865914	-872.7877713
	ΔE_0 (kJ/mol)		-3.0978
	μ (Debye)	12.1218 D	10.4978 D
	$\Delta E_1[^1B_u^+]$ (eV)	1.476	1.305
	$\Delta\Delta E_1(cm^{-1})$	1379.20	

A2-ethyl syn	Property	6-s-cis	6-s-trans
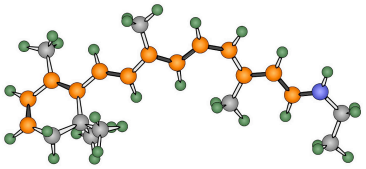	E_0 (Hartree)	-912.1022548	-912.1033805
	ΔE_0 (kJ/mol)		-2.9553
	μ (Debye)	11.2412 D	9.7806 D
	$\Delta E_1[^1B_u^+]$ (eV)	1.597	1.405
	$\Delta\Delta E_1(cm^{-1})$	1548.58	

A2-methyl PSB with water	Property	6-s-cis	6-s-trans
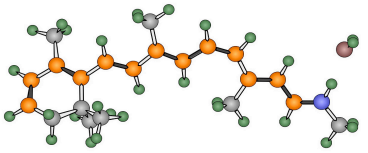	E_0 (Hartree)	-949.2164011	-949.2173656
	ΔE_0 (kJ/mol)		-2.5322
	μ (Debye)	14.8141 D	13.2687 D
	$\Delta E_1[^1B_u^+]$ (eV)	1.635	1.439
	$\Delta\Delta E_1(cm^{-1})$	1580.84	

A2-asp up	Property	6-s-cis	6-s-trans
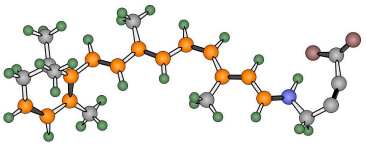	E_0 (Hartree)	-1137.026897	-1137.0265942
	ΔE_0 (kJ/mol)	-0.7950	
	μ (Debye)	19.8241 D	20.8899 D
	$\Delta E_1[^1B_u^+]$ (eV)	2.784	2.530
	$\Delta\Delta E_1(cm^{-1})$	2048.64	

A2-asp down with water	Property	6-s-cis	6-s-trans
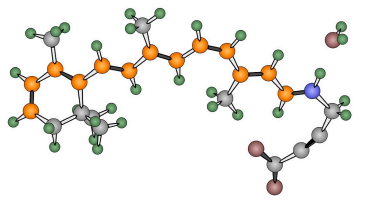	E_0 (Hartree)	-1213.4594536	-1216.4590649
	ΔE_0 (kJ/mol)		-7875.47
	μ (Debye)	17.9494 D	18.1190 D
	$\Delta E_1[^1B_u^+]$ (eV)	2.554	2.320
	$\Delta\Delta E_1(cm^{-1})$	1887.33	

Table S4 continued

A2-asp up with water	Property	6-s-cis	6-s-trans
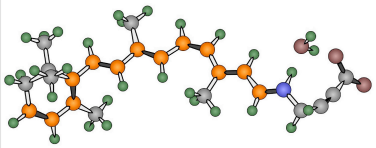	E_0 (Hartree)	-1213.4758777	-1213.4756560
	ΔE_0 (kJ/mol)	-0.5820	
	μ (Debye)	22.9928 D	23.0115 D
	$\Delta E_1[^1B_u^+]$ (eV)	2.581	2.333
	$\Delta\Delta E_1(cm^{-1})$	2000.25	

A2-perchlorate	Property	6-s-cis	6-s-trans
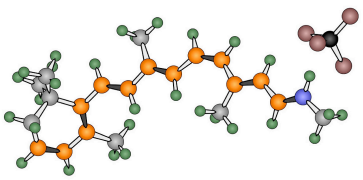	E_0 (Hartree)	-1633.7088133	-1633.70740533
	ΔE_0 (kJ/mol)	-3.6966	
	μ (Debye)	17.3596 D	17.8056 D
	$\Delta E_1[^1B_u^+]$ (eV)	2.525	2.357
	$\Delta\Delta E_1(cm^{-1})$	1355.01	

A2-9-NH_2 asp up	Property	6-s-cis	6-s-trans
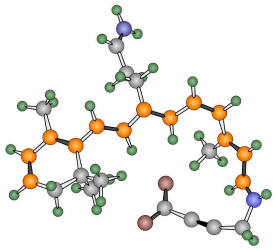	E_0 (Hartree)	-1270.1476897	-1270.1559854
	ΔE_0 (kJ/mol)		-21.7803
	μ (Debye)	28.0813 D	22.9090 D
	$\Delta E_1[^1B_u^+]$ (eV)	2.543	2.207
	$\Delta\Delta E_1(cm^{-1})$	2710.02	

A2-perchlorate with 2 waters	Property	6-s-cis	6-s-trans
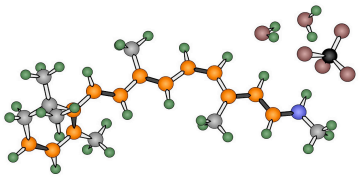	E_0 (Hartree)	-1786.5735044	-1786.5731929
	ΔE_0 (kJ/mol)	-0.8178	
	μ (Debye)	15.8846 D	16.7425 D
	$\Delta E_1[^1B_u^+]$ (eV)	2.497	2.247
	$\Delta\Delta E_1(cm^{-1})$	2016.38	

A2-9-glu asp up	Property	6-s-cis	6-s-trans
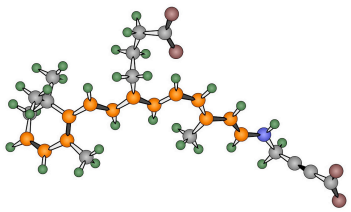	E_0 (Hartree)	-1403.6731944	-1403.6716429
	ΔE_0 (kJ/mol)	-4.0734	
	μ (Debye)	35.1945 D	35.7364 D
	$\Delta E_1[^1B_u^+]$ (eV)	2.255	2.229
	$\Delta\Delta E_1(cm^{-1})$	209.70	

Table S5: Comparison of residues at positions 164, 261, and 269 in selected red cone pigments found in regions 1 and 3 for the histogram of Figure 3.

A1 M/LWS	**λ_{max} (in nm)**	**Residue 164**	**Residue 261**	**Residue 269**
Region 1				
Mouse	510	Ala	Tyr	Thr
Guinea Pig	516	Ser	Tyr	Ala
Rabbit	520	Ala	Tyr	Thr
Bottle-nosed Dolphin	524	Ala	Tyr	Thr
Human Green	531	Ala	Phe	Ala
Region 3				
Cavefish	558	Ser	Tyr	Thr
Human Red	560	Ser	Tyr	Thr
Zebrafinch	560	Ser	Tyr	Thr
Iodopsin	570	Ser	Tyr	Thr
Canary	571	Ser	Tyr	Thr

REFERENCES

(29) Frisch, M. J., Trucks, G. W., Schlegel, H. B., Scuseria, G. E., Robb, M., Cheeseman, J. R., Montgomery Jr., Vreven, T., Kudin, K. N., Burant, J. C., Millam, J. M., Iyengar, S. S., Tomasi, J., Barone, V., Mennucci, B., Cossi, M., Scalmani, G., Rega, N., Petersson, G. A., Nakatsuji, H., Hada, M., Ehara, M., Toyota, K., Fukuda, R., Hasegawa, J., Ishida, M., Nakajima, T., Honda, Y., Kitao, O., Nakai, H., Klene, M., Li, X., Knox, J. E., Hratchian, H. P., Cross, J. B., Adamo, C., Jaramillo, J., Gomperts, R., Stratmann, R. E., Yazyev, O., Austin, A. J., Cammi, R., Pomelli, C., Ochterski, J., Ayala, P. Y., Morokuma, K., Voth, G. A., Salvador, P., Dannenberg, J. J., Zakrzewski, V. G., Dapprich, S., Daniels, A. D., Strain, M. C., Farkas, O., Malick, D. K., Rabuck, A. D., Raghavachari, K., Foresman, J. B., Ortiz, J. V., Cui, Q., Baboul, A. G., Clifford, S., Cioslowski, J., Stefanov, B. B., Liu, G., Liashenko, A., Piskorz, P., Komaromi, I., Martin, R. L., Fox, D. J., Keith, T. A., Al-Laham, M. A., Peng, C. Y., Nanayakkara, A., Challacombe, M., Gill, P. M. W., Johnson, B., Chen, W., Wong, M. W., Gonzalez, C., and Pople, J. A. (2003) Gaussian 03. *Gaussian, Inc., Pittsburgh PA*.

(30) Shima, S., Ilagan, R. P., Gillespie, N., Sommer, B. J., Hiller, R. G., Sharples, F. P., Frank, H. A., and Birge, R. R. (2003) Two-photon and fluorescence spectroscopy and the effect of environment on the photochemical properties of peridinin in solution and in the peridinin-chlorophyll-protein from Amphidinium carterae. *J. Phys. Chem. A. 107*, 8052 - 8066.

(31) Kusnetzow, A. K., Dukkipati, A., Babu, K. R., Ramos, L., Knox, B. E., and Birge, R. R. (2004) Vertebrate ultraviolet visual pigments: protonation of the retinylidene Schiff base and a counterion switch during photoactivation. *Proc. Natl. Acad. Sci. USA 101*, 941-6.

(32) Martin, C. H., and Birge, R. R. (1998) Reparameterizing MNDO for excited state calculations using ab initio effective Hamiltonian theory: Application to the 2,4-pentadien-1-iminium cation. *J. Phys. Chem. A 102*, 852-860.

(33) Ren, L., Martin, C. H., Wise, K. J., Gillespie, N. B., Luecke, H., Lanyi, J. K., Spudich, J. L., and Birge, R. R. (2001) Molecular mechanism of spectral tuning in sensory rhodopsin II. *Biochemistry 40*, 13906-13914.

(34) Szel, A., and Rohlich, P. (1988) Four photoreceptor types in the ground squirrel retina as evidenced by immunocytochemistry. *Vision Res. 28*, 1297-302.

(35) Ebrey, T., and Koutalos, Y. (2001) Vertebrate photoreceptors. *Prog. Retinal Eye Res. 20*, 49-94.

(36) Hart, N. S. (2001) The visual ecology of avian photoreceptors. *Progress in Retinal and Eye 20*, 675-703.

(37) Whitmore, A. V., Bowmaker, J.K. (1989) Seasonal variation in cone sensitivity and short-wave absorbing visual pigment in the rudd Scardinius erythrophthalmus. *J. Comp. Phys. A 166*, 103-115.

(38) Sun, H., Macke, J. P., and Nathans, J. (1997) Mechanisms of spectral tuning in the mouse green cone pigment. *Proc. Natl. Acad. Sci. U.S.A. 94*, 8860-8865.

(39) Lyubarsky, A. L., Falsini, B., Pennesi, M. E., Valentini, P., and Pugh, E. N. (1999) UV- and midwave-sensitive cone-driven retinal responses of the mouse: A possible

phenotype for coexpression of cone photopigments. *Journal of Neuroscience 19*, 442-455.

(40) Bowmaker, J. K., Govardovskii, V. I., Shukolyukov, S. A., Zueva, L. V., Hunt, D. M., Sideleva, V. G., and Smirnova, O. G. (1994) Visual pigments and the photic environment: the cottoid fish of Lake Baikal. *Vision Res. 34*, 591-605.

(41) Britt, L. L., Loew, E. R., and McFarland, W. N. (2001) Visual pigments in the early life stages of Pacific northwest marine fishes. *Journal of Experimental Biology 204*, 2581-2587.

(42) Harosi, F. I. (1994) An analysis of two spectral properties of vertebrate visual pigments. *Vision Res. 34*, 1359-1367.

(43) Yokoyama, S., and Radlwimmer, F. B. (1999) The molecular genetics of red and green color vision in mammals. *Genetics 153*, 919-932.

(44) Evans, B. I., Harosi, F. I., and Fernald, R. D. (1993) Photoreceptor spectral absorbance in larval and adult winter flounder (Pseudopleuronectes americanus). *Vis. Neurosci. 10*, 1065-1071.

(45) Loew, E. R., Govardovskii, V. I., Rohlich, P., and Szel, A. (1996) Microspectrophotometric and immunocytochemical identification of ultraviolet photoreceptors in geckos. *Vis. Neurosci. 13*, 247-256.

(46) Loew, E. R. (1994) A third, ultraviolet-sensitive, visual pigment in the Tokay gecko (Gekko gekko). *Vision Res. 34*, 1427-31.

(47) Shand, J., Archer, M. A., Thomas, N., and Cleary, J. (2001) Retinal development of West Australian dhufish, Glaucosoma hebraicum. *Vis. Neurosci. 18*, 711-24.

(48) Fasick, J. I., and Robsinson, P. R. (1998) Mechanism of spectral tuning in the dolphin visual pigments. *Biochemistry 37*, 433-438.

(49) Barry, K. L., and Hawryshyn, C. W. (1999) Spectral sensitivity of the Hawaiian saddle wrasse, Thalassoma duperrey, and implications for visually mediated behaviour on coral reefs. *Environmental Biology of Fishes 56*, 429-442.

(50) Cummings, M. E., and Partridge, J. C. (2001) Visual pigments and optical habitats of surfperch (Embiotocidae) in the California kelp forest. *Journal of comparative physiology. A, Neuroethology, sensory, neural, and behavioral physiology 187*, 875-889.

(51) Bowmaker, J. K., and Kunz, Y. W. (1985) The visual pigments of the weever fish, Trachinus vipera: a microspectrophotometric study. *Experimental biology 44*, 139-145.

(52) Yokoyama, S., and Radlwimmer, F. B. (2001) The molecular genetics and evolution of red and green color vision in vertebrates. *Genetics 158*, 1697-1710.

(53) Jacobs, G. H., Deegan, J. F., 2nd, and Moran, J. L. (1996) ERG measurements of the spectral sensitivity of common chimpanzee (Pan troglodytes). *Vision Res. 36*, 2587-2594.

(54) Parry Juliet, W. L., and Bowmaker James, K. (2002) Visual pigment coexpression in Guinea pig cones: a microspectrophotometric study. *Investigative Ophthalmology and Visual Science 43*, 1662-1665.

(55) Okano, T., Fukada, Y., and Yoshizawa, T. (1995) Molecular basis for tetrachromatic color vision. *Comparative Biochemistry and Physiology, B: Biochemistry and Molecular Biology 112B*, 405-414.

(56) Deeb Samir, S., Wakefield Matthew, J., Tada, T., Marotte, L., Yokoyama, S., and Marshall Graves Jenny, A. (2003) The Cone Visual Pigments of an Australian Marsupial, the Tammar Wallaby (Macropus eugenii): Sequence, Spectral Tuning, and Evolution. *Molecular Biology and Evolution 20*, 1642-1649.
(57) Bowmaker, J. K., Astell, S., Hunt, D. M., and Mollon, J. D. (1991) Photosensitive and photostable pigments in the retinae of Old World monkeys. *Journal of Experimental Biology 156*, 1-19.
(58) Hawryshyn, C. W., Haimberger, T. J., and Deutschlander, M. E. (2001) Microspectrophotometric measurements of vertebrate photoreceptors using CCD-based detection technology. *Journal of Experimental Biology 204*, 2431-2438.
(59) Neitz, M., Neitz, J., and Jacobs, G. H. (1991) Spectral tuning of pigments underlying red-green color vision. *Science (Washington, DC, United States) 252*, 971-974.
(60) McFarland, W. N., and Loew, E. R. (1994) Ultraviolet visual pigments in marine fishes of the family pomacentridae. *Vision Res. 34*, 1393-1396.
(61) Archer, S. N., and Lythgoe, J. N. (1990) The visual pigment basis for cone polymorphism in the guppy, Poecilia reticulata. *Vision Res. 30*, 225-33.
(62) Carleton, K. L., and Kocher, T. D. (2001) Cone opsin genes of African cichlid fishes: tuning spectral sensitivity by differential gene expression. *Molecular Biology and Evolution 18*, 1540-1550.
(63) David-Gray, Z. K., Cooper, H. M., Janssen, J. W. H., Nevo, E., and Foster, R. G. (1999) Spectral tuning of a circadian photopigment in a subterranean 'blind' mammal (Spalax ehrenbergi). *FEBS Letters 461*, 343-347.
(64) Shand, J., Hart Nathan, S., Thomas, N., and Partridge Julian, C. (2002) Developmental changes in the cone visual pigments of black bream Acanthopagrus butcheri. *Journal of Experimental Biology 205*, 3661-3667.
(65) Arrese Catherine, A., Hart Nathan, S., Thomas, N., Beazley Lyn, D., and Shand, J. (2002) Trichromacy in Australian marsupials. *Current Biology 12*, 657-60.
(66) Bowmaker, J. K., Jacobs, G. H., Spiegelhalter, D. J., and Mollon, J. D. (1985) Two types of trichromatic squirrel monkey share a pigment in the red-green spectral region. *Vision Res. 25*, 1937-1946.
(67) Parry, J. W. L., Peirson, S. N., Wilkens, H., and Bowmaker, J. K. (2003) Multiple photopigments from the Mexican blind cavefish, Astyanax fasciatus: a microspectrophotometric study. *Vision Res. 43*, 31-41.
(68) Jacobs, G. H., Deegan, J. F., 2nd, and Neitz, J. (1998) Photopigment basis for dichromatic color vision in cows, goats, and sheep. *Vis. Neurosci. 15*, 581-584.
(69) Carroll, J., Murphy, C. J., Neitz, M., Hoeve, J. N., and Neitz, J. (2001) Photopigment basis for dichromatic color vision in the horse. *Journal of Vision 1*, 80-7.
(70) Blakeslee, B., and Jacobs, G. H. (1985) Color Vision in the Ring-Tailed Lemur (Lemur catta). *Brain Behavior Evolution 26*, 154-166.
(71) Jacobs, G. H., Deegan, J. F., 2nd, Crognale, M. A., and Fenwick, J. A. (1993) Photopigments of dogs and foxes and their implications for canid vision. *Vis. Neurosci. 10*, 173-180.

(72) Jacobs, G. H., and Deegan, J. F., 2nd. (2003) Cone pigment variations in four genera of new world monkeys. *Vision Res. 43*, 227-236.
(73) Jacobs, G. H., and Neitz, J. (1987) Polymorphism of the middle wavelength cone in two species of South American monkey: Cebus apella and Callicebus moloch. *Vision Res. 27*, 1263-1268.
(74) Chinen, A., Hamaoka, T., Yamada, Y., and Kawamura, S. (2003) Gene duplication and spectral diversification of cone visual pigments of zebrafish. *Genetics 163*, 663-675.
(75) Sillman, A. J., Johnson, J. L., and Loew, E. R. (2001) Retinal photoreceptors and visual pigments in Boa constrictor imperator. *Journal of Experimental Zoology 290*, 359-65.
(76) Sillman, A. J., Carver, J. K., and Loew Ellis, R. (1999) The photoreceptors and visual pigments in the retina of a boid snake, the ball python (Python Regius). *The Journal of Experimental Biology 202*, 1931-1938.
(77) Petry, H. M., and Harosi, F. I. (1990) Visual pigments of the tree shrew (Tupaia belangeri) and greater galago (Galago crassicaudatus): a microspectrophotometric investigation. *Vision Res. 30*, 839-851.
(78) Hart, N. S., Partridge, J. C., Cuthill, I. C., and Bennett, A. T. (2000) Visual pigments, oil droplets, ocular media and cone photoreceptor distribution in two species of passerine bird: the blue tit (Parus caeruleus L.) and the blackbird (Turdus merula L.). *J. Comp. Phys. A 186*, 375-387.
(79) Kawamura, S., and Yokoyama, S. (1998) Functional characterization of visual and nonvisual pigments of American chameleon (Anolis carolinensis). *Vision Res. 38*, 37-44.
(80) Palacios, A. G., Goldsmith, T. H., and Bernard, G. D. (1996) Sensitivity of cones from a cyprinid fish (Danio aequipinnatus) to ultraviolet and visible light. *Vis. Neurosci. 13*, 411-421.
(81) Yokoyama, S. (2000) Phylogenetic analysis and experimental approaches to study color vision in vertebrates. *Methods Enzymol. 315*, 312-325.
(82) Flamarique, I. N., and Harosi, F. I. (2000) Photoreceptors, visual pigments, and ellipsosomes in the killifish, Fundulus heteroclitus: a microspectrophotometric and histological study. *Vis. Neurosci. 17*, 403-420.
(83) Hart, N. S., Partridge, J. C., Bennett, A. T., and Cuthill, I. C. (2000) Visual pigments, cone oil droplets and ocular media in four species of estrildid finch. *J. Comp. Phys. A 186*, 681-694.
(84) Cameron David, A. (2002) Mapping absorbance spectra, cone fractions, and neuronal mechanisms to photopic spectral sensitivity in the zebrafish. *Vis. Neurosci. 19*, 365-372.
(85) Barbour Helen, R., Archer Michael, A., Hart Nathan, S., Thomas, N., Dunlop Sarah, A., Beazley Lyn, D., and Shand, J. (2002) Retinal characteristics of the ornate dragon lizard, Ctenophorus ornatus. *J. Comp. Neurol. 450*, 334-44.
(86) Makino, C. L., Groesbeek, M., Lugtenburg, J., and Baylor, D. A. (1999) Spectral tuning in salamander visual pigments studied with dihydroretinal chromophores. *Biophys. J. 77*, 1024-1035.

(87) Loew, E. R., and Govardovskii, V. I. (2001) Photoreceptors and visual pigments in the red-eared turtle, Trachemys scripta elegans. *Vis. Neurosci. 18*, 753-757.
(88) Collin Shaun, P., Hart Nathan, S., Shand, J., and Potter Ian, C. (2003) Morphology and spectral absorption characteristics of retinal photoreceptors in the southern hemisphere lamprey (Geotria australis). *Vis. Neurosci. 20*, 119-130.
(89) Sillman, A. J., O'Leary, C. J., Tarantino, C. D., and Loew, E. R. (1999) The photoreceptors and visual pigments of two species of Acipenseriformes, the shovelnose sturgeon (Scaphirhynchus platorynchus) and the paddlefish (Polyodon spathula). *J. Comp. Phys. A 184*, 37-47.
(90) Harosi, F. I., and Kleinschmidt, J. (1993) Visual pigments in the sea lamprey, Petromyzon marinus. *Vis. Neurosci. 10*, 711-715.
(91) Kleinschmidt, J., and Harosi, F. I. (1992) Anion sensitivity and spectral tuning of cone visual pigments in situ. *Proc. Natl. Acad. Sci. U.S.A. 89*, 9181-9185.
(92) Cameron, D. A., Cornwall, M. C., and MacNichol, E. F., Jr. (1997) Visual pigment assignments in regenerated retina. *Journal of Neuroscience 17*, 917-923.
(93) Loew, E. R., and Lythgoe, J. N. (1978) The ecology of cone pigments in teleost fishes. *Vision Res. 18*, 715-722.
(94) Bowmaker, J. K., and Kunz, Y. W. (1987) Ultraviolet receptors, tetrachromatic colour vision and retinal mosaics in the brown trout (Salmo trutta): age-dependent changes. *Vision Res. 27*, 2101-8.
(95) Govardovskii, V. I., Fyhrquist, N., Reuter, T., Kuzmin, D. G., and Donner, K. (2000) In search of the visual pigment template. *Vis. Neurosci. 17*, 509-528.
(96) Sillman, A. J., Sorsky, M. E., and Loew, E. R. (1995) The Visual Pigments of Wild White Sturgeon (Acipenser-Transmontanus). *Canadian Journal of Zoology-Revue Canadienne De Zoologie 73*, 805-809.
(97) Miller, J. L., and Korenbrot, J. I. (1993) Phototransduction and adaptation in rods, single cones, and twin cones of the striped bass retina: a comparative study. *Vis. Neurosci. 10*, 653-667.
(98) Govardovskii, V. I., Rohlich, P., Szel, A., and Zueva, L. V. (1992) Immunocytochemical reactivity of rod and cone visual pigments in the sturgeon retina. *Vis. Neurosci. 8*, 531-537.
(99) Govardovskii, V. I., Byzov, A. L., Zueva, L. V., Polisczuk, N. A., and Baburina, E. A. (1991) Spectral characteristics of photoreceptors and horizontal cells in the retina of the Siberian sturgeon Acipenser baeri Brandt. *Vision Res. 31*, 2047-2056.
(100) Loew, E. R., and Wahl, C. M. (1991) A short-wavelength sensitive cone mechanism in juvenile yellow perch, Perca flavescens. *Vision Res. 31*, 353-360.